REVIEWS

Journal of Semiconductors
(2020) 41, 051202
doi: 10.1088/1674-4926/41/5/051202

HI hydrolysis-derived intermediate as booster for $CsPbI_3$ perovskite: from crystal structure, film fabrication to device performance

Zhizai Li and Zhiwen Jin†

School of Physical Science and Technology & Key Laboratory for Magnetism and Magnetic Materials (MoE) & Key Laboratory of Special Function Materials and Structure Design (MoE) & National & Local Joint Engineering Laboratory for Optical Conversion Materials and Technology, Lanzhou University, Lanzhou 730000, China

Abstract: Nowadays, inorganic $CsPbI_3$ perovskite solar cells (PSCs) have become one of the most attractive research hotspots in photovoltaic field for its superior chemical stability and excellent photo-electronic properties. Since the first independent report in 2015, the power conversion efficiency (PCE) of $CsPbI_3$ based PSCs has sharply increased from 3.9% to 19.03%. Importantly, during the developing process of $CsPbI_3$ PSCs, HI hydrolysis-derived intermediate plays an important role: from stabilizing the crystal structure, optimizing the fabricated film to boosting the device performance. In this review, the different crystal and electronic structures of $CsPbI_3$ are introduced. We then trace the history and disputes of HI hydrolysis-derived intermediate to make this review more logical. Meanwhile, we highlight the functions of HI hydrolysis-derived intermediate, and systematically summarize the advanced works on $CsPbI_3$ PSCs. Finally, the bottlenecks and prospects are revealed to further increase the $CsPbI_3$ PSCs performance.

Key words: $CsPbI_3$; HI; intermediate; crystal structure; stability

Citation: Z Z Li and Z W Jin, HI hydrolysis-derived intermediate as booster for $CsPbI_3$ perovskite: from crystal structure, film fabrication to device performance[J]. *J. Semicond.*, 2020, 41(5), 051202. http://doi.org/10.1088/1674-4926/41/5/051202

1. Introduction

Since the first organic–inorganic hybrid perovskite solar cell (PSCs) was proposed by Miyasaka's group[1], its power conversion efficiency (PCE) has sky-rocketed from 3.8% to 25.2% over the past decade[2–4]. This quick growth rate has made it as a hotspot in recent years because of its fascinating properties, such as high absorption coefficient[5, 6], low exciton binding energy[7–9], tunable band gap[10, 11], long carrier diffusion length[12, 13], and superb carrier mobility[14, 15]. Though great progresses have been achieved in term of its PCE, there still exist some problems. Volatility and hygroscopic A-site cations decompose the perovskite structure under extreme environment and destroy the performance of the device[16–21].

$CsPbX_3$ is a promising candidate to conquer these problems because Cs^+ is the most feasible inorganic cation to replay volatility and hygroscopic A-site with suitable tolerance factor[22–26]. Besides, the structures of organic cation (e.g., $CH_3NH_3^+$) have orientation freedom, while Cs^+ is symmetric without a multiple structure, which make hybrid perovskites show an unstable structure under extreme environments[27–31]. Among all of the $CsPbX_3$ materials, $CsPbI_3$ with a bandgap of ~1.7 eV is a suitable and promising candidate for high performance and stable output photovoltaic material[32–34].

$CsPbI_3$ has four different phases (cubic (α), tetragonal (β), orthorhombic (γ) and non-perovskite yellow (δ) phase) and each phase transforms under different temperatures[35]. At room temperature (RT), $CsPbI_3$ will finally transfer into non-perovskite phase (δ-phase) with an unsuitable bandgap of 2.75 eV, which limits its practical application[36–38]. Many researchers have conducted a series of methods to conquer this problem[39–41]. In the $CsPbI_3$ PSCs development process, HI hydrolysis-derived intermediate plays an important role[42–44]: stabilizing the crystal structure, optimizing the fabricated film and improving the device performance.

In this review, we aim to summarize the latest works about $CsPbI_3$ PSCs based on HI hydrolysis-derived intermediate. First, we briefly review the different crystal and electronic structures of $CsPbI_3$. We then trace the history and disputes of HI hydrolysis-derived intermediate to make this review more logical. Afterward, we highlight the functions of HI hydrolysis-derived intermediate, and systematically summarize some advanced works about HI hydrolysis-derived intermediate on $CsPbI_3$ PSCs. Finally, present issues and outlines are discussed to further increase the $CsPbI_3$ PSCs performance.

2. Crystal/electronic structure

Photo-electric properties (e.g., optical transitions, charger transfer) are greatly related to crystal and electronic properties (e.g., phase transition, energy band)[45–47]. In this section, we mainly discuss the $CsPbI_3$ perovskite from two aspects: crystal structure and electronic structure.

2.1. Crystal structure

The $CsPbI_3$ perovskite structure can be described as: Pb-site and I-site ion form a corner sharing $[PbI_6]^{4-}$ octahedron, while the Cs cation resides in the cuboctahedral cavities[48, 49]. There are mainly four types of structures: cubic structure (α,

Correspondence to: Z W Jin, jinzw@lzu.edu.cn
Received 4 FEBRUARY 2020; Revised 23 FEBRUARY 2020.

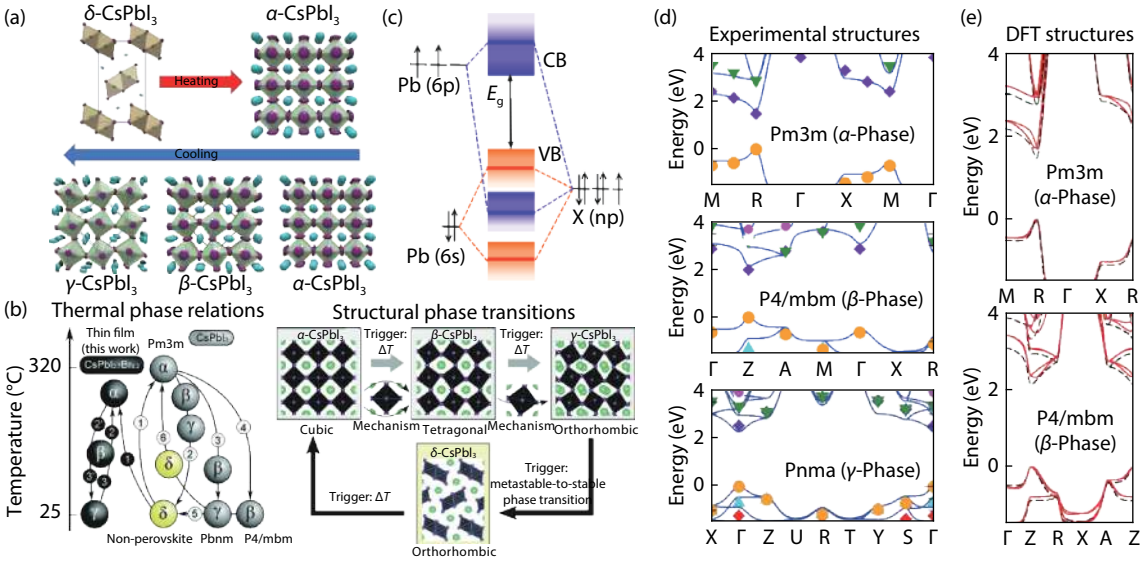

Fig. 1. (Color online) (a) The structure and transition of $CsPbI_3$ phases versus temperature. Reproduced with permission[46]. Copyright 2018, American Chemical Society Publications. (b) The transition of $CsPbI_3$ thermal phase and their transition mechanism. Reproduced with permission[35]. Copyright 2019, Science Publishing Group. (c) Schematic of bonding/antibonding orbitals in $CsPbX_3$. Reproduce with permission[54]. Copyright 2016, American Chemical Society Publications. (d) Electronic band structure of $CsPbI_3$ calculated by DFT and (e) tight-binding model. Reproduced with permission[46]. Copyright 2018, American Chemical Society Publications.

Pm $\bar{3}$m), tetragonal structure (β, P4/mbm), orthorhombic structure (γ, Pbnm), and non-perovskite phase (δ, Pnma)[46], as shown in Fig. 1(a). $CsPbI_3$ possesses an unsuitable Goldschmidt tolerance factor (t) in the range of 0.81–0.84, which is smaller than the ideal value (t, 0.9–1) and leads an unstable perovskite structure[50]. The transitions of each phase in different temperatures are shown in Fig. 1(b)[35].

The detailed transition temperature between each phase was researched by Even *et al.*, based on density functional theory (DFT) analyzation. The increasing thermal parameters of I^- tended to strength the dynamic motion of the corner-connected $[PbI_{6/2}]^-$ octahedral, which further induced a change of the unit cell volume and made δ-phase transformed to α-phase at 595 K. Then, with dynamic states gradually relaxing, α-phase transitions to β-phase at 539 K; β-phase transitions to γ-phase at 425 K; finally γ-phase turns to yellow non-perovskite phase (δ-phase) at RT[46].

The different stability of each phases can be ascribed to the different dissociated energies. The dissociation energy from $CsPbI_3$ to CsI and PbI_2 for α-, γ-, and δ-phase are 0.04, –0.09 and –0.16 eV, respectively. δ-phase $CsPbI_3$ shows a small Pb–I–Pb bond angel (95.09° and 91.40°) than α-phase $CsPbI_3$ (180°) and γ-phase $CsPbI_3$ (154.74°), which reduces the orbital overlap between Pb and I atoms and also makes δ-phase $CsPbI_3$ with a deeper defect transition energy level than α-, γ-phase. This indicates that δ-phase is the most stable phase because of its lowest dissociation energy[51]. Most importantly, different cooling rates change the formation energies for $CsPbI_3$ phases. α-phase converts to γ-phase when rapidly cooled in dry air, while slowly cooling leads to δ-phase phase because of different formation energies[52]. Besides, changing the temperature to cause the structure transition, a polar solvent also induces lattice distortion in $CsPbI_3$. A polar solvent would induce the lattice distortion of $CsPbI_3$ nanocubes by triggering the dipole moment, which leads to the self-assembly from α-$CsPbI_3$ to a γ-phase through oriented attachment process[53]. These studies indicate that metastable phases (contained β, γ-phase $CsPbI_3$) are more promising than α-$CsPbI_3$.

2.2. Electronic structure

The valence band maximum (VBM) of $CsPbI_3$ perovskite is constituted of antibonding hybridized Pb 6s and X np orbitals, among which X np takes the lead. However, Pb 6p is in the dominant place of conduction band minimum (CBM), as shown in Fig. 1(c)[54]. Compared with organic A-site cations, Cs^+ has little effect on $CsPbI_3$ electronic properties. A-site cations could indirectly influence perovskite electronic properties through Coulombic interactions and steric hindrance to deform the perovskite lattice, which makes perovskite electronic structure close to the band edges and further changes the band gap energetics[55].

The calculated electronic of α-, β- and γ-$CsPbI_3$ are depicted in Figs. 1(d) and 1(e)[46]. According to the tight-binding (TB) and DFT structures, taking band folding into account, we can vividly draw that all the different band gaps of $CsPbI_3$ phases are direct, and the band gap of α-$CsPbI_3$ shifts from the R point in the Brillouin zone to Z and Γ for β-$CsPbI_3$ and γ-$CsPbI_3$, respectively. This change indicates that the electronic band gap gradually increases with the transition from α-$CsPbI_3$ to more distorted β- and γ-$CsPbI_3$ because the $[PbI_6]^{4-}$ rotations stabilize the top of VBM and destabilize the bottom of CBM[56].

3. The functions of HI hydrolysis-derived intermediate

We summarize the performance of $CsPbI_3$ PSCs after introducing HI hydrolysis-derived intermediate in Table 1 (sPCE is the stable PCE). Its main functions can be summarized as following:

1) Reducing crystallization energy barrier in low temperature fabrication;

Table 1. Photovoltaic parameters of $CsPbI_3$ PSCs fabricated by HI hydrolysis-derived intermediate.

Material	Configuration	J_{SC} (mA/cm^2)	V_{OC} (V)	FF (%)	PCE (%)	sPCE (%)	Ref.
α-phase $CsPbI_3$	ITO/PEDOT:PSS/$CsPbI_3$/PCBM/BCP/LiF/Al	8.17	0.870	69.0	4.88	–	[62]
	ITO/PEDOT:PSS/$CsPbI_3$/PCBM/BCP/LiF/Al	5.89	0.960	64.0	3.66	–	[63]
	FTO/TiO_2/$CsPbI_3$·xEDAPbI_4/Spiro/Ag	14.53	1.150	71.0	11.86	–	[78]
	FTO/TiO_2/$CsPbI_3$/Carbon	18.50	0.790	65.0	9.50	–	[68]
	ITO/SnO_2/LiF/$CsPbI_{3-x}Br_x$/Spiro/Au	18.30	1.234	82.6	18.64	–	[70]
	FTO/TiO_2/$CsPbI_{3-x}$-DETAI_3/P3HT/Au	12.21	1.060	61.0	7.89	–	[67]
	FTO/PTAA/OTG3-$CsPbI_3$/PCBM/BCP/Ag	15.81	1.120	75.2	13.32	13.20	[80]
	FTO/TiO_2/PEAI-$CsPbI_3$/Spiro/Ag	18.40	1.110	69.6	14.30	13.50	[79]
Metastable (β- and γ-) phase $CsPbI_3$	FTO/TiO_2/$CsPbI_3$/PTAA/Au	18.95	1.059	74.9	15.07	–	[43]
	FTO/NiO*x*/STCG-$CsPbI_3$/ZnO/ITO	18.29	1.090	80.5	16.04	–	[84]
	FTO/TiO_2/$CsPbI_3$/PTAA/Au	19.75	1.135	76.6	17.17	16.83	[86]
	N-CQDs EDS/FTO/TiO_2/$CsPbI_3$/PTAA/Au	19.15	1.106	75.6	16.02	15.90	[89]
	FTO/TiO_2/$CsPbI_3$/PTAA/Au	18.31	1.110	78.0	15.91	–	[85]
	FTO/TiO_2/$CsPbI_3$/PTAA/Au	20.34	1.090	77.0	17.03	–	[88]
	FTO/TiO_2/$CsPbI_3$/PTAA/Au	21.15	1.090	77.0	17.30	16.78	[76]
	FTO/TiO_2/$CsPbI_3$/P3HT/Au	16.53	1.040	65.7	11.30	9.70	[83]
	FTO/TiO_2/$CsPbI_3$/PTAA/Au	19.58	1.084	75.7	16.07	15.47	87]
	FTO/TiO_2/$CsPbI_3$/UCNP-PTAA/Au	19.17	1.113	74.3	15.86	15.59	[90]
	FTO/TiO_2/$CsPbI_3$/PTAA/Au	20.30	1.080	75.5	16.24	–	[91]
Low dimension $CsPbI_3$	FTO/TiO_2/$CsPbI_3$/PTAA/Au	19.51	0.993	70.5	13.65	13.29	[98]
	ITO/PTAA/$CsPbI_3$/C_{60}/BCP/Cu	17.21	1.090	67.5	12.65	–	[101]
	ITO/SnO_2/$CsPbI_3$/Spiro/Au	16.59	1.070	70.0	12.40	–	[97]
	FTO/TiO_2/$CsPbI_3$/Carbon	15.76	0.910	66.0	9.39	–	[99]
$DMA_xCs_{1-x}PbI_3$	FTO/TiO_2/$DMA_{0.15}Cs_{0.85}PbI_3$/Spiro/Ag	19.40	1.050	75.0	15.30	–	[75]
	FTO/TiO_2/DMAI-$CsPbI_3$/Spiro/Ag	20.23	1.137	82.7	19.03	–	[74]
	FTO/TiO_2/$Cs_{0.5}DMA_{0.5}PbI_3$/Spiro/Ag	18.40	1.054	74.0	14.30	–	[72]
	ITO/PEDOT:PSS/$Cs_{0.7}DMA_{0.3}PbI_3$/C_{60}/BCP/Ag	16.65	0.990	76.5	12.62	–	[71]
	FTO/TiO_2/DMAI-$CsPbI_3$/Spiro/Ag	20.23	1.110	82.0	18.40	–	[73]

2) Increasing iodide coordination numbers to decrease structural disorder, modifying structure and forming higher-order iodoplumbate complexes;

3) Slowing down the rapid crystalline process and obtaining high-quality $CsPbI_3$ film;

4) Inducing strain to generate distorted metastable phase (β- and γ- $CsPbI_3$);

5) Modifying the band gap of perovskites films.

4. History and disputes of HI hydrolysis-derived intermediate

The solution one-step method has advantages of simple, convenience and facile process, and can also be compatible roll-to-roll fabrication technology[57]. However, the one-step deposition process shows poor morphology and low performance because of the rapid reaction in the solution. The common solution is using intermediates to slow down the quick reaction and make it controllable. However, understanding the composition of the HI hydrolysis-derived intermediate still needs a long time.

4.1. HI

In the early stage, researchers focused on using HI additive in $CsPbI_3$ PSCs fabrication to cause a microstrain and induce a low temperature phase transition process. Meanwhile, extra halides in HI precursor solution tended to fill the vacancies of perovskites, resulting in change of metal–halogen–metal bond connectivity, and consequently cell volumes and optical bandgap[58]. Besides, PbI_2 first coordinated with DMF in the precursor through Pb–O bonds, but further added HI would eliminate PbI_2–DMF coordination and form higher-order iodoplumbate complexes (e.g., PbI_4^{2-}, PbI_5^{3-}, and PbI_6^{4-}), which benefited the formation of high-quality $CsPbI_3$ film[59, 60].

In 2015, HI was first used as an additive in $CsPbI_3$ PSCs. Snaith *et al.* introduced a small amount of HI in the precursor solution before spin-coating. They found that HI additive could change the solubility of precursor materials and induce a strain to lower the temperature phase transition. Then, strain triggered small crystals appearing and significantly stabilized its structure in RT, as shown in Fig. 2(a)[42]. Uddin *et al.* controlled the concentration of HI on purpose to modify $CsPbI_3$ bandgap. They demonstrated that introducing 36 μL/mL HI would decrease the bandgap from 1.75 eV to optimized value of 1.7 eV and show excellence electronic properties with low charge-transport (12.8 kΩ). From the scanning electron microscopy (SEM) images, optimal concentration HI additive led to the appearance of small grain sizes with a few nanometers, which is beneficial to increase the stability of black phase $CsPbI_3$[61]. This conclusion was also proven by Kim *et al.*, who found that HI formed small grains and stabilized the black phase of $CsPbI_3$ at low temperature[62]. Furthermore, they investigated the function of NH_4^+ (e.g., NH_4Cl, NH_4Br and NH_4I) and H^+ (HCl, HBr and HI) based additive and found that HI additive is the most efficient, and which could reduce the roughness and increase the stability of perovskites films. In particular, when it was exposed in ambient for 3 h, the optimal device with $CsPbI_3$ perovskite only dropped its PCE from 3.55% to 2.78%[63].

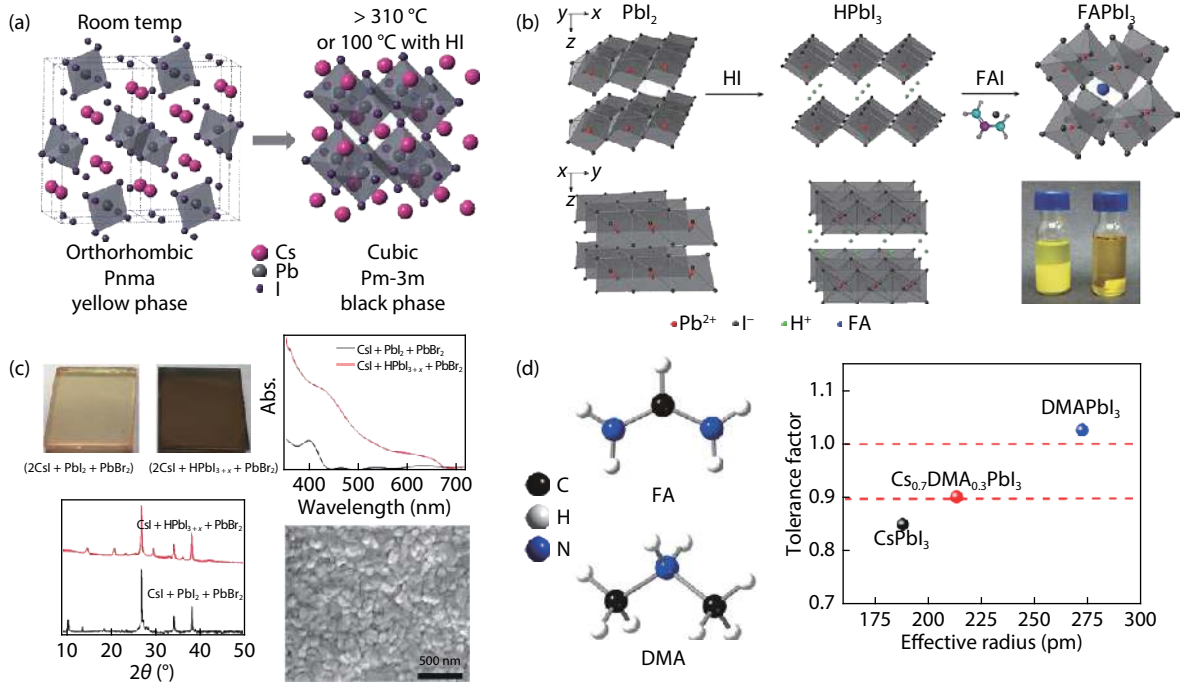

Fig. 2. (Color online) (a) The diagrammatic of HI fabricated $CsPbI_3$. Reproduced with permission[42]. Copyright 2015, The Royal Society of Chemistry. (b) Schematic of using $HPbI_3$ to fabricate $FAPbI_3$ PSCs. Reproduced with permission[65]. Copyright 2015, Wiley-VCH Publications. (c) Detail information of PbI_2 and $HPbI_3$ fabricated perovskite film. Reproduced with permission[69]. Copyright 2018, Wiley-VCH Publications. (d) The molecular structure of FA and DMA, and the tolerance factor of corresponding perovskite ($CsPbI_3$, $Cs_{0.7}DMA_{0.3}PbI_3$ and $DMAPbI_3$). Reproduced with permission[71]. Copyright 2018, Nature Publishing Group.

4.2. PbI_2·*x*HI or $HPbI_3$

In addition to HI additive, HI hydrolysis-derived intermediate is more effective because it eliminates water in the HI solution and is an intermediate compound to increase perovskite crystallinity[64]. It was first proposed in 2015 by Zhao *et al.* They developed a new precursor compound (named $HPbI_3$) through a reaction of HI and PbI_2 in DMF solution, and used it to replace PbI_2 in fabrication $FAPbI_3$-based PSCs, as shown in Fig. 2(b)[65]. Such $HPbI_3$ has a pseudo-3D crystal structure, where 1D face-shared $[PbI_6]^{4-}$ octahedra with intercalated protons (H^+) for charge balance[66].

Zhu *et al.* introduced $HPbI_3$ into the $CsPbI_3$ PSCs and assisted with a triple cation $NH_3^+C_2H_4NH_2^+C_2H_4NH_3^+$ (named as $DETA^{3+}$) to further stabilize the α-$CsPbI_3$ perovskite phases[67]. Subsequently, Chen *et al.* used $HPbI_3$ to substitute PbI_2 and found that tensile lattice strain appeared in $HPbI_3$-process $CsPbI_3$ perovskite[68]. The tensile lattice strain generated because $HPbI_3$ crystals serve as a template to guide the nucleation and growth of α-$CsPbI_3$. A similar work was conducted by Zhao *et al.*, who introduced the I-excess precursor $HPbI_{3+x}$ and replace PbI_2 to reduce crystallization energy barrier, and fabricated α-$CsPbI_{3-x}Br_x$ PSCs in low temperature (130 °C). The champion PCE of 13.61% was measured by a reverse scanning, as shown in Fig. 2(c)[69]. More recently, in order to overcome the low PCE problem of $CsPbI_3$-based PSC, You *et al.* used CsI, $HPbI_{3+x}$ and $PbBr_2$ as precursor to fabricate high-quality $CsPbI_{3-x}Br_x$ perovskite films. They developed an inorganic shunt-blocking layer lithium fluoride (LiF) in the ETL/perovskite interface to align the bandgap and suppress the surface defect. Furthermore, a small amount of $PbCl_2$ were introduced to further suppress the recombination. Finally, they obtained $CsPbI_{3-x}Br_x$ with the highest PCE of 18.64%, and boosted V_{OC} to 1.25 V with little loss. After continuous 1 sun equivalent illumination, the best device dropped only 6% of its initial PCE after 1000 h[70].

4.3. PbI_2·*x*DMAI or $DMAPbI_3$

Kanatzidis *et al.* recently claimed that $HPbI_3$ did not exist and was replaced by a compound of $DMAPbI_3$, which generated through DMF hydrolysis in HI solution. Importantly, they pointed out that some early reports of inorganic perovskite are actually the hybrid perovskite. They found that $DMAPbI_3$ possessed a larger tolerance factor and mixing with Cs^+ could adjust tolerance factor (*t*) of the compounds ($Cs_{1-x}DMA_xPbI_3$) toward an ideal factor (*t*, 0.9–1). Finally, they achieved a champion PCE of 12.62% in $Cs_{1-x}DMA_xPbI_3$-based PSCs, as shown in Fig. 2(d)[71]. Liu *et al.* dissolved PbI_2 and HI in DMF to synthesize $DMAPbI_3$ and further confirmed that no $HPbI_3$ existed. They used it as precursor to fabricate high-quality $Cs_xDMA_{1-x}PbI_3$ perovskite films with 14.3% PCE, and the initial PCE kept more than 85% when exposed in air 20 days without encapsulation, as shown in Fig. 3(a)[72].

Zhao *et al.* used PbI_2·*x*DMAI to fabricate $CsPbI_3$ PSCs recently, and they concluded that the fabricated perovskites are actually all inorganic composition because the organic ion DMA^+ are easily lost during the high-temperature (210 °C) annealing process[73]. Later, they proved that DMAI is a volatile additive, and used it to assist with phenyltrimethylammonium chloride (PTACl) passivation. Finally, they obtained the highest PCE of $CsPbI_3$ PSC, 19.03%, as shown in Fig. 3(b)[74]. This conclusion was also confirmed by Pang *et al.*, who found that $DMAPbI_3$ and Cs_4PbI_6 first formed in annealing 100 °C for 10 min. When the annealing temperature was increased to

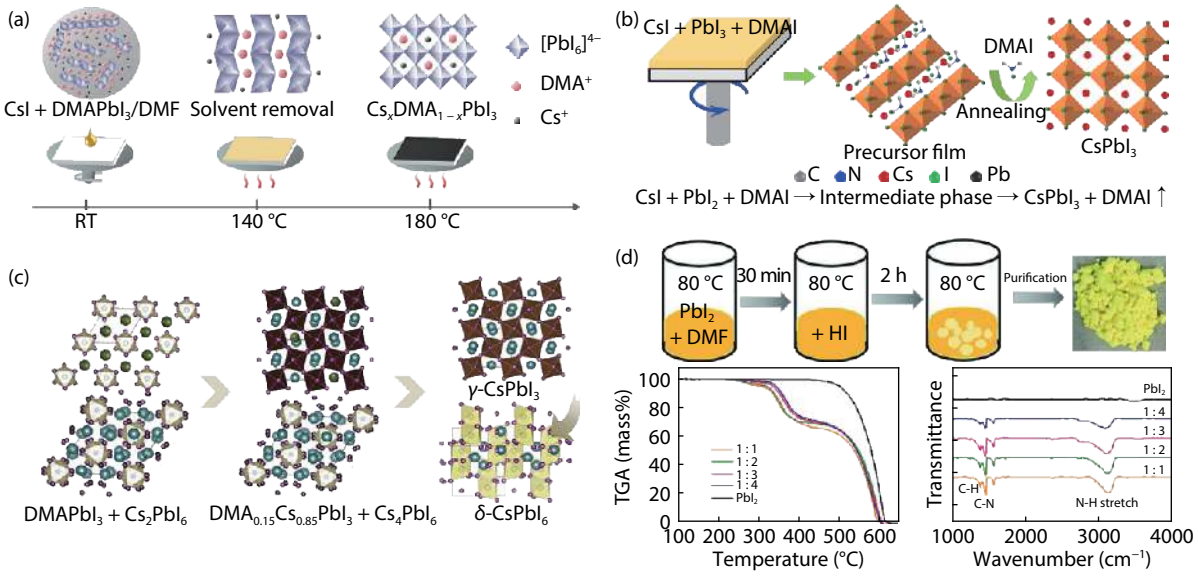

Fig. 3. (Color online) (a) Schematic illustration the fabrication process of $Cs_xDMA_{1-x}PbI_3$. Reproduced with permission[72]. Copyright 2019, Elsevier Inc Publications. (b) Schematic diagram of using DMAI additive to form $CsPbI_3$ films. Reproduced with permission[74]. Copyright 2019, Wiley-VCH Publications. (c) The changeable component of DMAI-fabricated perovskite versus annealing temperature. Reproduced with permission[75]. Copyright 2020, American Chemical Society Publications. (d) Schematic diagram of $DMAPbI_3$ synthesis process and the information of corresponding perovskite. Reproduced with permission[76]. Copyright 2019, Wiley-VCH Publications.

180 °C for 15 min, $DMAPbI_3$ converted into $DMA_{0.15}Cs_{0.85}PbI_3$ with a small amount Cs_4PbI_6 residue. Once the annealing temperature exceeded 200 °C, the γ-phase $CsPbI_3$ was formed with a small number of $DMA_{0.15}Cs_{0.85}PbI_3$ residue. The number of $DMA_{0.15}Cs_{0.85}PbI_3$ greatly decreased and a little δ-phase appeared, as shown in Fig. 3(c)[75].

Our groups also confirmed this conclusion. We synthesized a series of intermediate compounds (DMAI and $DMAPbI_3$) by different ratio of HI/DMF, and used them to fabricate $CsPbI_3$ PSCs. After detailed analysis, we found that the major component of $CsPbI_3$ was still inorganic in this reaction route. Most of DMA^+ organic molecules lost during the annealing process, and only a small amount of DMA^+ remained to stabilize perovskite structure. Excessive DMA^+ interacted with Pb^{2+} to further passivate $CsPbI_3$ surface, as shown in Fig. 3(d)[76].

In conclusion, the organic molecule DMAI mainly influence the crystallization kinetics and perovskite phase. During the annealing process, DMAI will sublimate quickly, change the rate of crystallization and form metastable (β- and γ-) phase based $CsPbI_3$. The controllable crystallization kinetics and stable (β- and γ-) phase are beneficial to morphology and stability of perovskite, respectively. Besides, DMA^+ (2.72 Å) possesses a larger ionic radius than Cs^+ (1.88 Å)[77]. Therefore, if the DMA^+ is residual (non-sublimate) in the $CsPbI_3$ film: (1) DMA^+ doped into the lattice of $CsPbI_3$ can increase its tolerance factor for avoiding crystal structure distortion; (2) DMA^+ reacted with Pb^{2+} to passivate $CsPbI_3$ surface, further reducing leakage current generation for increasing the device performance.

5. Applying HI hydrolysis-derived intermediate in $CsPbI_3$ PSCs

5.1. α-phase $CsPbI_3$ based PSCs

As we discussed earlier, HI hydrolysis-derived intermediate showed a lot of advantages in high-quality film fabrication and device performance. Importantly, perovskite films with better crystallinity, morphology, and higher range of absorption are the foundation of efficiency.

The first working α-$CsPbI_3$ PSCs with a PCE of 2.9% was fabricated in low temperature (100 °C) by Snaith and his cooperators via a small amount HI additive adding[42]. Many relevant works have been done to boost its performance. Uddin *et al.*[61] and Kim *et al.*[62] used HI to modify the α-$CsPbI_3$ film morphology and boost its PCE to 6.44% and 4.88%, respectively. Later, Zhao *et al.* discovered that $PbI_2.xHI$ could reduce the crystallization energy barrier for α-$CsPbI_3$ phase. They used $PbI_2.xHI$ assist with two-dimension $EDAPbI_4$ perovskite to stabilize α-$CsPbI_3$ phase and avoid lattice distortion. Finally, α-$CsPbI_3$ phase based on the $EDAPbI_4$ passivation showed a record PCE of 11.8% together with superior stability, as shown in Fig. 4(a). The α-$CsPbI_3$ phase perovskite kept its structure after annealing at 100 °C for more than 150 h and stable at RT for months[78].

Compared with HI, the absence of H_2O molecules in HI hydrolysis-derived intermediate can optimize the perovskite crystallinity and morphology. Chen and his cooperators replaced PbI_2 with $HPbI_3$ in fabricating stable α-$CsPbI_3$ film. They found that the bandgap was shifted from 1.72 to 1.68 eV owing to formation of tensile lattice strain. Finally, a HTL free α-$CsPbI_3$ was obtained with a higher PCE of 9.5%. Besides, the optimal device showed enhanced stability, which maintained 90% of its initial PCE under illumination for more than 3000 h in dry environment, as shown in Fig. 4(b)[68]. Then, organic terminal groups were widely used to assist $HPbI_3$ and further improve α-phase $CsPbI_3$ stability. Zhu *et al.* introduced $DETA^{3+}$ additive into the $HPbI_3$ containing precursor to stabilize α-$CsPbI_3$ perovskite phases. $DETA^{3+}$ has NH_3^+ or RHN_2^+ group, which could combine with I^- or $[PbI_6]^{4-}$ and avoid octahedral tilting. Besides, oil-wet (hydrophobic) hydrocarbon chains of $DETA^{3+}$

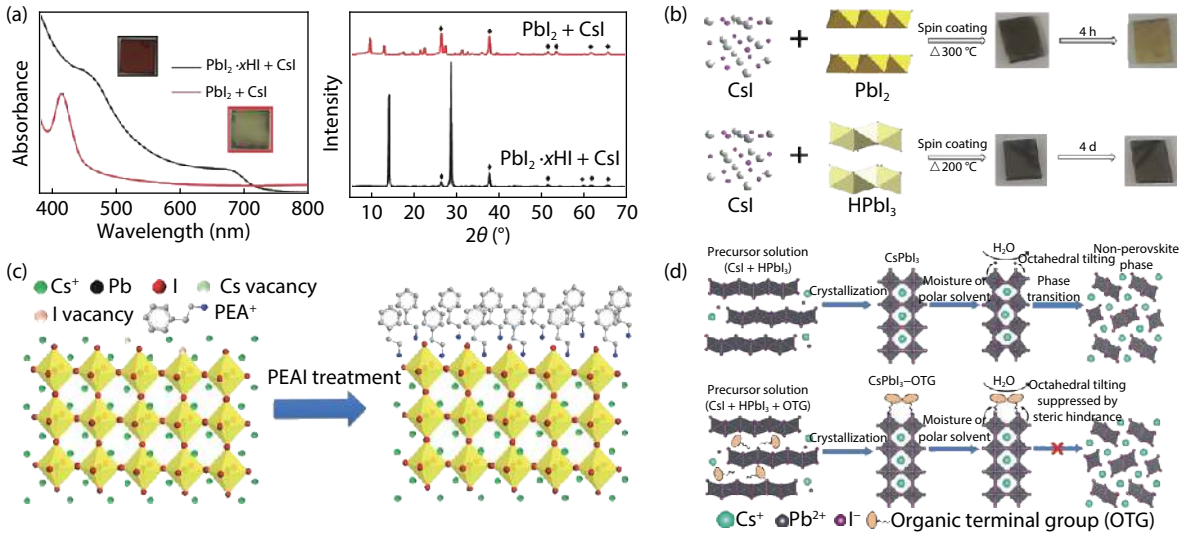

Fig. 4. (Color online) (a) The detail information of PbI_2·HI and PbI_2 fabricated perovskite, inserted pictures are their digital photos. Reproduced with permission[78]. Copyright 2017, Wiley-VCH Publications. (b) The diagram of PbI_2 and $HPbI_3$ fabricated $CsPbI_3$ film, respectively. Reproduced with permission[68]. Copyright 2018, American Chemical Society Publications. (c) Schematic of PEA^+ organic ligand treatment on $CsPbI_3$ thin film. Reproduced with permission[79]. Copyright 2018, Elsevier Inc Publications. (d) Diagram illustrates the mechanism of with/without OTG passivation. Reproduced with permission[80]. Copyright 2019, Wiley-VCH Publications.

increased the $CsPbI_3$ humidity-resistance. Ultimately, the optimal device kept its structure for more than 6 h in a humid environment (~30 °C, 60%–70% RH), while the reference device changed its color from black to yellow in the same condition in 55 min, indicating a phase transition[67]. Zhao *et al.* fabricated $HPbI_{3+x}$ to form α-$CsPbI_3$ perovskite film. With the help of PEAI post-treated on the α-$CsPbI_3$, superior PCE of 13.5% was obtained with improved stability. Because of PEA^+ terminated on the $CsPbI_3$ surface and did as a capping layer, PEA^+-$CsPbI_3$ remained stable structure after 80 °C annealing for 7 days, while the pure one degraded into non-perovskite in the same condition, as shown in Fig. 4(c)[79] . Han *et al.* added organic terminal groups (OTG) into CsI and $HPbI_3$ precursors to design an inverted planar $CsPbI_3$ PSCs. They report that OTG induced a steric hindrance and suppressed octahedral $[PbI_6]^{4-}$ tilting. Moreover, OTG passivated the surface electronic traps states to further increase its performances. Finally, the inverted planar OTG-$CsPbI_3$ PSCs showed the highest PCE of 13.2% and retained about 85% of its initial PCE for 30 days at RT, while the reference device degraded completely in 3 weeks, as shown in Fig. 4(d)[80].

5.2. Metastable (β- and γ-) phase $CsPbI_3$ based PSCs

Recently, the $CsPbI_3$ films fabricated by HI hydrolysis-derived intermediate were proved metastable phases (combined β-phase $CsPbI_3$ with γ-phase $CsPbI_3$).

The β-phase $CsPbI_3$ can also be formed at low temperature and show more stable perovskite structure than α-phase one. However, it is difficult to deposit and stabilize its perovskite structure[81]. Zhao *et al.* adopted PbI_2·DMAI and CsI as precursor to fabricate stable β-phase $CsPbI_3$ with stable structure. Furthermore, they used choline iodine (CHI) to passiviate the surface trap states and aligned the energy level in the TiO_2/β-phase interface. β-phase $CsPbI_3$ PSCs has a particularly high PCE of 18.4% with distinguished ambient stability because of PbI_2·DMAI and CHI. The stability of β-$CsPbI_3$ PSCs were greatly improved: it retained 92% of its initial PCE after 500 h illumination at the maximum power point, as shown in Fig. 5(a)[73].

The γ-phase $CsPbI_3$ is the most stable black phase because of its lowest dissociation energy[82]. Hence, γ-phase $CsPbI_3$ was systematically researched to boost its stability and performance. Hu *et al.* used HI to fabricate high-quality $CsPbI_3$ film. After that, they introduced a small amount of H_2O into precursor to induce a proton transfer process in $CsPbI_3$ film, which could manipulate the grains size and improve stability of perovskite. When stored in ambient conditions, the optimal device showed no drop of its performance while the reference's PCE was greatly degraded, as shown in Fig. 5(b)[83]. Then, Nazeeruddin *et al.* developed a soft template-controlled growth method to fabricate pinhole-free γ-phase $CsPbI_3$ film, where (adamantan-1-yl)methanammonium (ADMA) acted as a template and ionized by HI. They pointed that ADMA absorbed on $CsPbI_3$ surface and induced a steric effect to further increase the nucleation rate at the initial stage of $CsPbI_3$ formation. Taking into account of controllable nucleation rate and excellent morphology, superior PCE of 16.04% was obtained with improved stability (drop only 10% after continuous light soaking and heating for 1000 h), as shown in Fig. 5(c)[84].

In our recent research, we reported the synergistic effect of HI and PEAI additives, where HI transferred to an intermediate ($HPbI_{3+x}$) to fabricate distorted black phase-based $CsPbI_3$ thin films and PEAI induced a steric effects to avoid phase transition. It is noteworthy that the best device maintained 92% of its initial PCE for 60 days storage in ambient (RH ~ 20%–30%, 25 °C), while the reference one degraded to 0.65% in the same condition for 8 days, as shown in Fig. 5(d)[43]. Then, $HPbI_3$ was used to fabricate $CsPbI_3$, assisted with anti-solvent hot substrate spin-coating method, and 15.91% PCE was obtained in a humidity environment (RH ~ 50%)[85]. Furthermore, we added a small amount of Br^- (5%) to the $HPbI_3$-$CsPbI_3$ lattice to increase phase stability by suppressing bulk trap-assisted non-radiative recombination and relaxing lat-

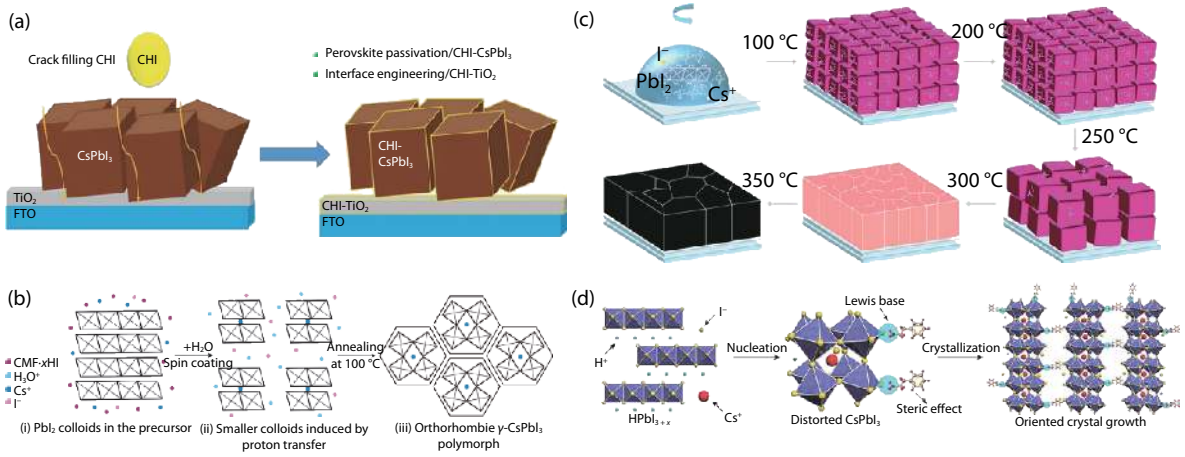

Fig. 5. (Color online) (a) Schematic illustration of CHI crack-filling interface engineering. Reproduced with permission[73]. Copyright 2019, Science Publishing Group. (b) Schematic diagram $CsPbI_3$ crystal formation by using HI and H_2O. Reproduced with permission[83]. Copyright 2018, American Chemical Society Publications. (c) Mechanism of STCG-$CsPbI_3$ film formation by assistant of ADMA molecule. Reproduced with permission[84]. Copyright 2020, Wiley-VCH Publications. (d) The schematic illustration of HI and PEAI do on the $CsPbI_3$. Reproduced with permission[43]. Copyright 2018, Nature Publishing Group.

tice strain. The performance was boost up to a record PCE of 17.17% together with excellent stability[86]. Another work we reported was that 3 mol% Cl^- was added to the γ-$CsPbI_3$ film with a 16.07% PCE obtained. It not only showed the excepted increase crystalline dynamics for an excellent $CsPbI_3$ morphology, but also improved crystalline orientation. The Cl-doping $CsPbI_3$ showed high stability, for optimal device dropped only 0.45% of its initial PCE under continuous light soaking for 200 h. More important, non-encapsulated $CsPbI_3$ PSCs with Cl^- doping degraded only 6% when stored in RH ~ 30% for 60 days (the fresh one dropped to 85% of its initial PCE in the same conditions)[87]. We also introduced 2% $Pb(SCN)_2$ into the $DMAPbI_3$ and CsI precursor to control the morphology of the $CsPbI_3$ film. In this case, a PCE of 17.04% with V_{OC} of 1.09 V was obtained[88].

One of the notorious problems to limit $CsPbI_3$ performance is the lower J_{SC} compared with hybrid one. Thus, we have also developed several strategies to increase its J_{SC}, such as harvesting short wavelength ultraviolet light (UV-light) or near-infrared (NIR) light, and designing device structure to capture light. First, we developed a downconversion nanoparticles (DCNPs) nitrogen-doped graphene quantum dots (N-GQDs) as an energy-down-shift to harvest the short wavelength (< 350 nm) UV-light. After combining it with $HPbI_3$-formed γ-$CsPbI_3$, the optimal device showed an improved short circuit current density (J_{SC}) from 18.67 to 19.15 mA/cm^2, with an increase of 2.57%. Meanwhile, its performance was greatly increased 3.15%, from 15.53% to 16.02%[89]. Furthermore, we developed a core-shell-structured upconversion nanoparticles (UCNPs) to capture the NIR light, making it possible to obtain 15.86% PCE (noted that the improvement of PCE is negligible), J_{SC} = 19.17 mA/cm^2[90]. We also investigated the influence of different haze glass substrates, and used the optimized one to fabricate $CsPbI_3$ PSCs with 16.24% PCE. We found that the improvement came from scattering effect of FTO, refractive index and roughness of each layer[91].

5.3. Low dimension $CsPbI_3$ based PSCs

Reducing dimension can further increase the stability of $CsPbI_3$ PSCs because reducing materials dimension can lead to more symmetric crystal structure and show a smaller surface energy[92–96].

However, the poor solubility of CsX in the precursor solution would severely limited the thickness of $CsPbI_3$ film and influence the light absorption. Chen *et al.* used $HPbX_3$ and CsAc as new precursor to overcome the poor solubility of Cs^+ precursor and fabricate α-$CsPbX_3$ with optimal thickness. They introduced phenylethylammonium iodide (PEAI) to $HPbX_3$ and CsAc system and further controlled the dimension of $CsPbX_3$ from three dimension (3D) to two dimension (2D). Finally, a champion PCE of 12.4% in 2D $CsPbI_3$ perovskite was obtained, and maintained 93% of its initial PCE in ambient for 40 days, as shown in Fig. 6(a)[97]. Similarly, our group used $DMAPbI_3$ as a new precursor to fabricated γ-$CsPbI_3$ perovskite, and then we introduced a judicious amount of PEAI into the $DMAPbI_3$ contained precursor to convert γ-$CsPbI_3$ PSCs into a 2D Ruddlesden–Popper (RP) structure $(PEA)_2(Cs)_{n-1}Pb_nI_{3n+1}$ perovskite. And the optimal 2D RP PSCs with highest PCE of 13.65%, showed a similar charge extraction and carrier lifetime compared with the 3D samples. The thermostability was tested in N_2 filled glovebox. The superior 2D RP PSCs kept 88% of its initial PCE when stored at 80 °C for 15 days, while the reference 3D γ-$CsPbI_3$ degraded to 69%. Besides, 2D RP PSCs maintained its black color whereas 3D γ-$CsPbI_3$ appeared yellow phase in RH ~ 30% for 12 days, as shown in Fig. 6(b)[98]. In addition to PEAI, Chen *et al.* first introduced a novel dual ammonium cation piperazine-1,4-diium (PZD^+) to generate 2D RP $CsPbI_3$. It's noted that one of the ammonium groups coordinated with $[PbI_6]^{4-}$ octahedral, and another one interacted with I^- to balance charge. Finally, the optimized device achieved a PCE of 9.39% and maintained its performance without decomposition under heating at 100 °C for 24 h[99].

Pradhan *et al.* fabricated stable $CsPbI_3$ nanocrystals (NCs) with superior stability by using a higher temperature (260 °C) than usual (160 °C), and adding olelyamine (OLA) and HI respectively in the reaction process (noted that only OLA or HI are less efficient). Taking the NMR analyzation into account, they found that higher temperature helped the OLA^+ ligands

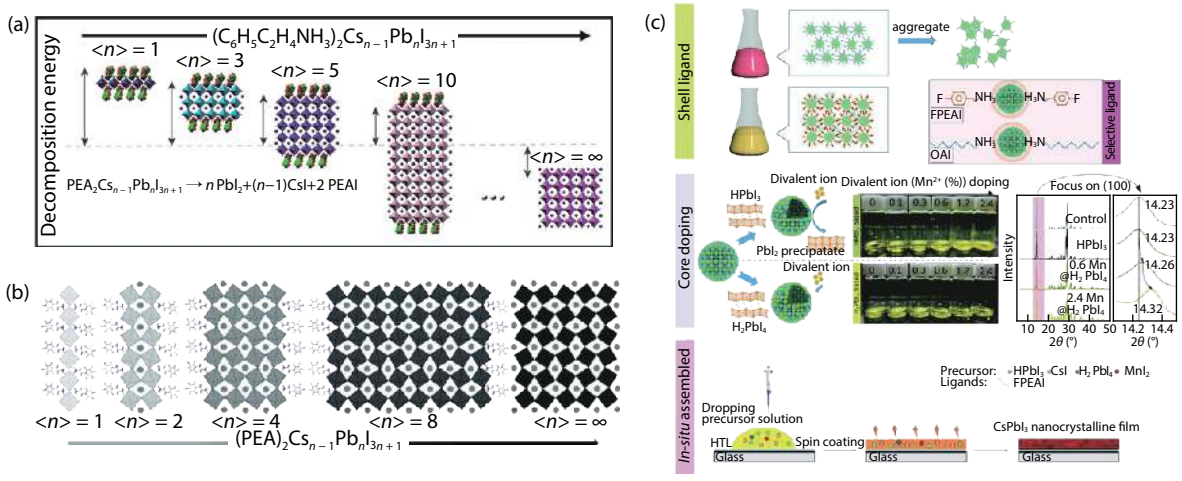

Fig. 6. (Color online) (a) The structure and decomposition energies of different n values $PEA_2Cs_{n-1}Pb_nX_{3n+1}$. Reproduced with permission[97]. Copyright 2018, Elsevier Inc Publications. (b) The controllable *n* values and structures of $PEA_2Cs_{n-1}Pb_nX_{3n+1}$. Reproduced with permission[98]. Copyright 2019, Wiley-VCH Publications. (c) Schematic illustration the fabrication process of shell ligand, $HPbI_3$, H_2PbI_4 and in-suit assembled of them. Reproduced with permission[101]. Copyright 2019, Wiley-VCH Publications.

to occupy the Cs^+ position on the surface and further stabilized its structure[100]. To solve adverse shell ligands and unstable core lattices in nanocrystals, Choi *et al.* developed a rational core-shell design method in $CsPbI_3$ NCs. They used a novel ligand named 4-fluorophenethylammonium iodide (FPEAI) to enhance the binding force between the ligand and $CsPbI_3$ NCs and efficient charge coupling between NCs, to increase charge extraction. Besides, H_2PbI_4, which was synthesized with excessive HI, was used to assist doping Mn^{2+} ion into perovskite lattices and to further raise the performance of $CsPbI_3$ NCs to 13.4% with superb stability (maintained 92% of its PCE in air for 500 h), as shown in Fig. 6(c)[101].

6. Prospects and outlook

Although lots of advanced works about HI hydrolysis-derived intermediate have been done to boost PCE of $CsPbI_3$ PSCs, its PCE still far behind the hybrid ones. Therefore, we need to analyze the urgent problems that remain and develop corresponding strategies to improve the performance of $CsPbI_3$ perovskites.

Increasing the light absorption. As we show in Table 1, though the performance of $CsPbI_3$ PSCs has reach 19.03%[74] , the J_{SC} (about 20 mA/cm^2) is still lower than the hybrid one. This maybe cause by current loss and insufficient utilization of light, resulting from the relatively large bandgap (compared with hybrid perovskite films). Developing high efficiency DCNPs/UCNPs, to capture UV-light or NIR could be an useful solution[90].

Doping X-site halide to improve $CsPbI_3$ PSCs stability. The unstable nature of $CsPbI_3$ is an unsuitable tolerance factor (*t*), as we mentioned earlier. Partially replacing I^- (2.2 Å) with smaller radius halides, e.g., Cl^- (1.87 Å) and Br^- (1.96 Å) or pseudohalide SCN^- (2.15 Å), could enlarge *t* value to reach ideal one (0.9–1)[32].

Ligand assists to stabilize $CsPbI_3$ crystal structure. Introducing ligand (e.g., OTG[80], poly-vinylpyrrolidone (PVP)[102], ADMA[84], PEAI[79], and DETA[67]) into a perovskite precursor and inducing a steric hindrance to further stable $CsPbI_3$ crystal structure is a useful way to boost its stability. Therefore, it is promising to develop and design new ligands.

Increasing the carrier transport for low dimension perovskite. Low dimension $CsPbI_3$ tends to increase surface-area-to-volume ratio and raise the Gibbs free energy to make the structure more stable[103]. It is noted that though low dimension $CsPbI_3$ can keep $CsPbI_3$ structure more stable, the PCE of low dimension $CsPbI_3$ is still far below the 3D $CsPbI_3$. Hence, we should pay more attention to increase the carrier transport for low dimension $CsPbI_3$.

Avoiding the disadvantage of intermediate. Liu *et al.* claimed that intermediates had negative influence during low dimension perovskite deposition process because they slowed down intercalation of ions and increased nucleation barrier, and further caused the byproduct formation[104]. Although there are no negative effects on HI hydrolysis-derived intermediate so far, we should be more vigilant against HI hydrolysis-derived intermediate.

In conclusion, $CsPbI_3$ perovskite, particularly the metastable phases (β- and γ-Phase $CsPbI_3$), is a promising material to replace the unstable hybrid perovskite. Besides, $CsPbI_3$ PSCs with suitable bandgap make it more suitable to apply in tandem solar cells and commercialization. Based on these advantages, we conclude that $CsPbI_3$ PSCs maybe the mainstream research direction in the near future, and we should adopt a positive attitude to it.

Acknowledgements

This work was funded by the National Natural Science Foundation of China (51902148, 61704099 and 51801088), the Fundamental Research Funds for the Central Universities (lzujbky-2020-61, lzujbky-2019-88 and lzujbky-2020-kb06), and the Special Funding for Open and Shared Large-Scale Instruments and Equipments of Lanzhou University (LZU-GXJJ-2019C023 and LZU-GXJJ-2019C019).

References

[1] Kojima A, Teshima K, Shirai Y, et al. Organometal halide perovskites as visible-light sensitizers for photovoltaic cells. J Am

Chem Soc, 2009, 131, 6050
[2] NREL. https://wwwnrelgov/pv/device-performancehtml. 2019
[3] Jiang J, Wang Q, Jin Z, et al. Polymer doping for high-efficiency perovskite solar cells with improved moisture stability. Adv Energy Mater, 2018, 8, 1701757
[4] Jiang J, Jin Z, Gao F, et al. $CsPbCl_3$-driven low-trap-density perovskite grain growth for > 20% solar cell efficiency. Adv Sci, 2018, 5, 1800474
[5] Wehrenfennig C, Eperon G E, Johnston M B, et al. High charge carrier mobilities and lifetimes in organolead trihalide perovskites. Adv Mater, 2014, 26, 1584
[6] Hu W, Cong H, Huang W, et al. Germanium/perovskite heterostructure for high-performance and broadband photodetector from visible to infrared telecommunication band. Light: Sci Appl, 2019, 8, 106
[7] D'Innocenzo V, Grancini G, Alcocer M J P, et al. Excitons versus free charges in organo-lead tri-halide perovskites. Nat Commun, 2014, 5, 3586
[8] Lin Q, Armin A, Nagiri R C R, et al. Electro-optics of perovskite solar cells. Nat Photon, 2014, 9, 106
[9] Fang H H, Wang F, Adjokatse S, et al. Photoexcitation dynamics in solution-processed formamidinium lead iodide perovskite thin films for solar cell applications. Light: Sci Appl, 2016, 5, e16056
[10] Noh J H, Im S H, Heo J H, et al. Chemical management for colorful, efficient, and stable inorganic –organic hybrid nanostructured solar cells. Nano Lett, 2013, 13, 1764
[11] Bian H, Bai D, Jin Z, et al. Graded bandgap $CsPbI_{2+x}Br_{1-x}$ perovskite solar cells with a stabilized efficiency of 14.4%. Joule, 2018, 2, 1500
[12] Stranks S D, Eperon G E, Grancini G, et al. Electron-hole diffusion lengths exceeding 1 micrometer in an organometal trihalide perovskite absorber. Science, 2013, 342, 341
[13] Wang H, Bian H, Jin Z, et al. Synergy of hydrophobic surface capping and lattice contraction for stable and high-efficiency inorganic $CsPbI_2Br$ perovskite solar cells. Solar RRL, 2018, 2, 1800216
[14] Stoumpos C C, Malliakas C D, Kanatzidis M G. Semiconducting tin and lead iodide perovskites with organic cations: phase transitions, high mobilities, and near-infrared photoluminescent properties. Inorg Chem, 2013, 52, 9019
[15] Zhao Y C, Zhou W K, Zhou X, et al. Quantification of light-enhanced ionic transport in lead iodide perovskite thin films and its solar cell applications. Light: Sci Appl, 2017, 6, e16243
[16] Xiao C, Li Z, Guthrey H, et al. Mechanisms of electron-beam-induced damage in perovskite thin films revealed by cathodoluminescence spectroscopy. J Phys Chem C, 2015, 119, 26904
[17] Akbulatov A F, Luchkin S Y, Frolova L A, et al. Probing the intrinsic thermal and photochemical stability of hybrid and inorganic lead halide perovskites. J Phys Chem Lett, 2017, 8, 1211
[18] Zhou W, Zhao Y, Zhou X, et al. Light-independent ionic transport in inorganic perovskite and ultrastable cs-based perovskite solar cells. J Phys Chem Lett, 2017, 8, 4122
[19] Wang Q, Zhang X, Jin Z, et al. Energy-down-shift $CsPbCl_3$:Mn quantum dots for boosting the efficiency and stability of perovskite solar cells. ACS Energy Lett, 2017, 2, 1479
[20] Jin Z, Yan J, Huang X, et al. Solution-processed transparent coordination polymer electrode for photovoltaic solar cells. Nano Energy, 2017, 40, 376
[21] Jiang J, Jin Z, Lei J, et al. ITIC surface modification to achieve synergistic electron transport layer enhancement for planar-type perovskite solar cells with efficiency exceeding 20%. J Mater Chem A, 2017, 5, 9514
[22] Beal R E, Slotcavage D J, Leijtens T, et al. Cesium lead halide perovskites with improved stability for tandem solar cells. J Phys Chem Lett, 2016, 7, 746
[23] Jia X, Zuo C, Tao S, et al. $CsPb(I_xBr_{1-x})_3$ solar cells. Sci Bull, 2019, 64, 1532
[24] Zhang X, Jin Z, Zhang J, et al. All-ambient processed binary $CsPbBr_3$-$CsPb_2Br_5$ perovskites with synergistic enhancement for high-efficiency Cs-Pb-Br-based solar cells. ACS Appl Mater Interfaces, 2018, 10, 7145
[25] Zhang J, Bai D, Jin Z, et al. 3D–2D–0D interface profiling for record efficiency all-inorganic $CsPbBrI_2$ perovskite solar cells with superior stability. Adv Energy Mater, 2018, 8, 1703246
[26] Bai D, Zhang J, Jin Z, et al. Interstitial Mn^{2+}-driven high-aspect-ratio grain growth for low-trap-density microcrystalline films for record efficiency $CsPbI_2Br$ solar cells. ACS Energy Lett, 2018, 3, 970
[27] Zhang Y Y, Chen S, Xu P, et al. Intrinsic instability of the hybrid halide perovskite semiconductor $CH_3NH_3PbI_3$. Chin Phys Lett, 2018, 35, 036104
[28] Kang C H, Dursun I, Liu G, et al. High-speed colour-converting photodetector with all-inorganic $CsPbBr_3$ perovskite nanocrystals for ultraviolet light communication. Light: Sci Appl, 2019, 8, 94
[29] Liu G, Zhou C, Wan F, et al. Dependence of power conversion properties of perovskite solar cells on operating temperature. Appl Phys Lett, 2018, 113, 3501
[30] Liu G, Yang B, Liu B, et al. Irreversible light-soaking effect of perovskite solar cells caused by light-induced oxygen vacancies in titanium oxide. Appl Phys Lett, 2017, 111, 3501
[31] Wang J F, Lin D X, Yuan Y B. Recent progress of ion migration in organometal halide perovskite. Acta Phys Sin, 2019, 68, 158801
[32] Ahmad W, Khan J, Niu G, et al. Inorganic $CsPbI_3$ perovskite-based solar cells: a choice for a tandem device. Solar RRL, 2017, 1, 1700048
[33] Wang P, Zhang X, Zhou Y, et al. Solvent-controlled growth of inorganic perovskite films in dry environment for efficient and stable solar cells. Nat Commun, 2018, 9, 2225
[34] Zhang X, Wang Q, Jin Z, et al. Stable ultra-fast broad-bandwidth photodetectors based on α-$CsPbI_3$ perovskite and $NaYF_4$:Yb,Er quantum dots. Nanoscale, 2017, 9, 6278
[35] Steele J A, Jin H D, Iurii I, et al. Thermal unequilibrium of strained black $CsPbI_3$ thin films. Science, 2019, 365, 679
[36] Hoffman J B, Schleper A L, Kamat P V. Transformation of sintered $CsPbBr_3$ nanocrystals to cubic $CsPbI_3$ and gradient $CsPbBr_xI_{3-x}$ through halide exchange. J Am Chem Soc, 2016, 138, 8603
[37] Wang Q, Jin Z, Chen D, et al. μ-graphene crosslinked $CsPbI_3$ quantum dots for high efficiency solar cells with much improved stability. Adv Energy Mater, 2018, 8, 1800007
[38] Zhao H, Xu J, Zhou S, et al. Preparation of tortuous 3D γ-$CsPbI_3$ films at low temperature by CaI_2 as dopant for highly efficient perovskite solar cells. Adv Funct Mater, 2019, 29, 1808986
[39] Dayan A S, Cohen B E, Aharon S, et al. Enhancing stability and photostability of $CsPbI_3$ by reducing its dimensionality. Chem Mater, 2018, 30, 8017
[40] Ye T, Zhou B, Zhan F, et al. Below 200 °C fabrication strategy of black phase $CsPbI_3$ film for ambient-air-stable solar cells. Solar RRL, 2019, 10
[41] Xiang S, Li W, Wei Y, et al. Natrium doping pushes the efficiency of carbon-based $CsPbI_3$ perovskite solar cells to 10.7%. iScience, 2019, 15, 156
[42] Eperon G E, Paternò G M, Sutton R J, et al. Inorganic caesium lead iodide perovskite solar cells. J Mater Chem A, 2015, 3, 19688
[43] Wang K, Jin Z, Liang L, et al. All-inorganic cesium lead iodide perovskite solar cells with stabilized efficiency beyond 15%. Nat Commun, 2018, 9, 4544
[44] Wang Y, Zhang T, Kan M, et al. Bifunctional stabilization of all-inorganic α-$CsPbI_3$ perovskite for 17% efficiency photovoltaics. J Am Chem Soc, 2018, 140, 12345
[45] Swarnkar A, Ravi V K, Nag A. Beyond colloidal cesium lead hal-

ide perovskite nanocrystals: analogous metal halides and doping. ACS Energy Lett, 2017, 2, 1089
[46] Marronnier A, Roma G, Boyer-Richard S, et al. Anharmonicity and disorder in the black phases of cesium lead iodide used for stable inorganic perovskite solar cells. ACS Nano, 2018, 12, 3477
[47] Bai D, Bian H, Jin Z, et al. Temperature-assisted crystallization for inorganic $CsPbI_2Br$ perovskite solar cells to attain high stabilized efficiency 14.81%. Nano Energy, 2018, 52, 408
[48] Green M A, Ho-Baillie A, Snaith H J. The emergence of perovskite solar cells. Nat Photon, 2014, 8, 506
[49] Eperon G E, Stranks S D, Menelaou C, et al. Formamidinium lead trihalide: a broadly tunable perovskite for efficient planar heterojunction solar cells. Energy Environ Sci, 2014, 7, 982
[50] Zhang J, Hodes G, Jin Z, et al. All-inorganic $CsPbX_3$ perovskite solar cells: progress and prospects. Angew Chem Int Ed, 2019, 58, 15596
[51] Huang Y, Yin W J, He Y. Intrinsic point defects in inorganic cesium lead iodide perovskite $CsPbI_3$. J Phys Chem C, 2018, 122, 1345
[52] Sutton R J, Filip M R, Haghighirad A A, et al. Cubic or orthorhombic? revealing the crystal structure of metastable black-phase $CsPbI_3$ by theory and experiment ACS Energy Lett, 2018, 3, 1787
[53] Sun J K, Huang S, Liu X Z, et al. Polar solvent induced lattice distortion of cubic $CsPbI_3$ nanocubes and hierarchical self-assembly into orthorhombic single-crystalline nanowires. J Am Chem Soc, 2018, 140, 11705
[54] Ravi V K, Markad G B, Nag A. Band edge energies and excitonic transition probabilities of colloidal $CsPbX_3$ (X = Cl, Br, I) perovskite nanocrystals. ACS Energy Lett, 2016, 1, 665
[55] Stoumpos C C, Kanatzidis M G. The renaissance of halide perovskites and their evolution as emerging semiconductors. Acc Chem Res, 2015, 48, 2791
[56] Katan C, Pedesseau L, Kepenekian M, et al. Interplay of spin–orbit coupling and lattice distortion in metal substituted 3D tri-chloride hybrid perovskites. J Mater Chem A, 2015, 3, 9232
[57] Zheng L, Zhang D, Ma Y, et al. Morphology control of the perovskite films for efficient solar cells. Dalton Trans, 2015, 44, 10582
[58] Soe C M M, Stoumpos C C, Harutyunyan B, et al. Room temperature phase transition in methylammonium lead iodide perovskite thin films induced by hydrohalic acid additives. ChemSusChem, 2016, 9, 2656
[59] Sharenko A, Mackeen C, Jewell L, et al. Evolution of iodoplumbate complexes in methylammonium lead iodide perovskite precursor solutions. Chem Mater, 2017, 29, 1315
[60] Mohamad D K, Freestone B G, Masters R, et al. Optimized organometal halide perovskite solar cell fabrication through control of nanoparticle crystal patterning. J Mater Chem C, 2017, 5, 2352
[61] Haque F, Wright M, Mahmud M A, et al. Effects of hydroiodic acid concentration on the properties of $CsPbI_3$ perovskite solar cells. ACS Omega, 2018, 3, 11937
[62] Kim Y G, Kim T Y, Oh J H, et al. cesium lead iodide solar cells controlled by annealing temperature. Phys Chem Chem Phys, 2017, 19, 6257
[63] Heo D Y, Han S M, Woo N S, et al. Role of additives on the performance of $CsPbI_3$ solar cells. J Phys Chem C, 2018, 122, 15903
[64] Wei Y, Li W, Xiang S, et al. Precursor effects on methylamine gas-induced $CH_3NH_3PbI_3$ films for stable carbon-based perovskite solar cells. Solar Energy, 2018, 174, 139
[65] Wang F, Yu H, Xu H, et al. $HPbI_3$: a new precursor compound for highly efficient solution-processed perovskite solar cells. Adv Funct Mater, 2015, 25, 1120
[66] Pang S, Zhou Y, Wang Z, et al. Transformative evolution of organolead triiodide perovskite thin films from strong room-temperature solid-gas interaction between $HPbI_3$–CH_3NH_2 precursor pair. J Am Chem Soc, 2016, 138, 750
[67] Ding X, Chen H, Wu Y, et al. Triple cation additive $NH_3^+C_2H_4NH_2^+C_2H_4NH_3^+$-induced phase-stable inorganic α-$CsPbI_3$ perovskite films for use in solar cells. J Mater Chem A, 2018, 6, 18258
[68] Xiang S, Fu Z, Li W, et al. Highly air-stable carbon-based α-$CsPbI_3$ perovskite solar cells with a broadened optical spectrum. ACS Energy Lett, 2018, 3, 1824
[69] Wang Y, Zhang T, Xu F, et al. A Facile low temperature fabrication of high performance $CsPbI_2Br$ all-inorganic perovskite solar cells. Solar RRL, 2018, 2, 1700180
[70] Ye Q, Zhao Y, Mu S, et al. Cesium lead inorganic solar cell with efficiency beyond 18% via reduced charge recombination. Adv Mater, 2019, 31, e1905143
[71] Ke W, Spanopoulos I, Stoumpos C C, et al. Myths and reality of $HPbI_3$ in halide perovskite solar cells. Nat Commun, 2018, 9, 4785
[72] Pei Y, Liu Y, Li F, et al. Unveiling property of hydrolysis-derived $DMAPbI_3$ for perovskite devices: composition engineering, defect mitigation, and stability optimization. iScience, 2019, 15, 165
[73] Wang Y, Dar M I, Ono L K, et al. Thermodynamically stabilized β-$CsPbI_3$–based perovskite solar cells with efficiencies >18%. Science, 2019, 365, 591
[74] Wang Y, Liu X, Zhang T, et al. the role of dimethylammonium iodide in $CsPbI_3$ perovskite fabrication: additive or dopant. Angew Chem Int Ed, 2019, 58, 16691
[75] Meng H, Shao Z, Wang L, et al. Chemical composition and phase evolution in DMAI-derived inorganic perovskite solar cells. ACS Energy Lett, 2020, 5, 263
[76] Bian H, Wang H, Li Z, et al. Unveiling the effects of hydrolysis-derived $DMAI/DMAPbI_x$ intermediate compound on performance of $CsPbI_3$ solar cells. Adv Sci, 2019, 10, 1902868
[77] Dutta A, Pradhan N. Phase-stable red-emitting $CsPbI_3$ nanocrystals: successes and challenges. ACS Energy Lett, 2019, 4, 709
[78] Zhang T, Dar M I, Li G, et al. Bication lead iodide 2D perovskite component to stabilize inorganic α-$CsPbI_3$ perovskite phase for high-efficiency solar cells. Adv Sci, 2017, 3, e1700841
[79] Wang Y, Zhang T, Kan M, et al. Efficient α-$CsPbI_3$ photovoltaics with surface terminated organic cations. Joule, 2018, 2, 2065
[80] Wu T, Wang Y, Dai Z, et al. Efficient and stable $CsPbI_3$ solar cells via regulating lattice distortion with surface organic terminal groups. Adv Mater, 2019, 31, e1900605
[81] Fu Y, Rea M T, Chen J, et al. Selective stabilization and photophysical properties of metastable perovskite polymorphs of $CsPbI_3$ in thin films. Chem Mater, 2017, 29, 8385
[82] Becker P, Márquez J A, Just J, et al. Low temperature synthesis of stable γ-$CsPbI_3$ perovskite layers for solar cells obtained by high throughput experimentation. Adv Energy Mater, 2019, 9, 1900555
[83] Zhao B, Jin S, Huang S, et al. Thermodynamically stable orthorhombic γ-$CsPbI_3$ thin films for high-performance photovoltaics. J Am Chem Soc, 2018, 140, 11716
[84] Liu C, Yang Y, Xia X, et al. Soft Template-controlled growth of high-quality $CsPbI_3$ films for efficient and stable solar cells. Adv Energy Mater, 2020, 10, 1903751
[85] Liang L, Zhizai L, Zhou F, et al. Humidity-insensitive fabrication of efficient $CsPbI_3$ solar cells in ambient air. J Mater Chem A, 2019, 7, 26776
[86] Wang H, Bian H, Jin Z, et al. Cesium lead mixed-halide perovskites for low-energy loss solar cells with efficiency beyond 17%. Chem Mater, 2019, 31, 6231
[87] Wang K, Jin Z, Liang L, et al. Chlorine doping for black γ-$CsPbI_3$ solar cells with stabilized efficiency beyond 16%. Nano Energy, 2019, 58, 175
[88] Yao Z, Jin Z, Zhang X, et al. Pseudohalide (SCN-)-doped $CsPbI_3$

for high performance solar cells. J Mater Chem C, 2019, 7, 13736
[89] Bian H, Wang Q, Yang S, et al. Nitrogen-doped graphene quantum dots for 80% photoluminescence quantum yield for inorganic γ-$CsPbI_3$ perovskite solar cells with efficiency beyond 16%. J Mater Chem A, 2019, 7, 5740
[90] Liang L, Liu M, Jin Z, et al. Optical Management with nanoparticles for a light conversion efficiency enhancement in inorganic γ-$CsPbI_3$ solar cells. Nano Lett, 2019, 19, 1796
[91] Bian H, Wang Q, Ding L, et al. Light management via tuning the fluorine-doped tin oxide glass haze-drives high-efficiency $CsPbI_3$ solar cells. Phys Status Solidi A, 2019, 216, 1900602
[92] Wang Q, Zheng X, Deng Y, et al. Stabilizing the α-phase of $CsPbI_3$ perovskite by sulfobetaine zwitterions in one-step spin-coating films. Joule, 2017, 1, 371
[93] Jin Z, Yuan M, Li H, et al. Graphdiyne: an efficient hole transporter for stable high-performance colloidal quantum dot solar cells. Adv Funct Mater, 2016, 26, 5284
[94] Jin Z, Wang A, Zhou Q, et al. Detecting trap states in planar PbS colloidal quantum dot solar cells. Sci Rep, 2016, 6, 37106
[95] Yao H, Zhou F, Li Z, et al. Strategies for improving the stability of tin-based perovskite ($ASnX_3$) solar cells. Adv Sci, 2020, 10, 1903540
[96] Jin Z, Zhou Q, Chen Y, et al. Graphdiyne:ZnO nanocomposites for high-performance UV photodetectors. Adv Mater, 2016, 28, 3697
[97] Jiang Y, Yuan J, Ni Y, et al. Reduced-dimensional α-$CsPbX_3$ perovskites for efficient and stable photovoltaics. Joule, 2018, 2, 1356
[98] Wang K, Li Z, Zhou F, et al. Ruddlesden–popper 2D component to stabilize γ-$CsPbI_3$ Perovskite phase for stable and efficient photovoltaics. Adv Energy Mater, 2019, 9, 1902529
[99] Wang H, Xiang S, Li W, et al. Skillfully deflecting the question: a small amount of piperazine-1,4-diium iodide radically enhances the thermal stability of $CsPbI_3$ perovskite. J Mater Chem C, 2019, 7, 11757
[100] Dutta A, Dutta S K, Das Adhikari S, et al. Phase-stable $CsPbI_3$ nanocrystals: the reaction temperature matters. Angew Chem Int Ed, 2018, 57, 9083
[101] Xi J, Piao C, Byeon J, et al. Rational core-shell design of open air low temperature in situ processable $CsPbI_3$ quasi-nanocrystals for stabilized p–i–n solar cells. Adv Energy Mater, 2019, 9, 1901787
[102] Li B, Zhang Y, Fu L, et al. Surface passivation engineering strategy to fully-inorganic cubic $CsPbI_3$ perovskites for high-performance solar cells. Nat Commun, 2018, 9, 1076
[103] Gan J, He J, Hoye R L Z, et al. α-$CsPbI_3$ colloidal quantum dots: synthesis, photodynamics, and photovoltaic applications. ACS Energy Lett, 2019, 4, 1308
[104] Zhang X, Munir R, Xu Z, et al. Phase transition control for high performance ruddlesden-popper perovskite solar cells. Adv Mater, 2018, 30, 1707166